ChemPubSoc Europe

DOI: 10.1002/chem.201802248

CHEMISTRY
A European Journal
Full Paper

Chemical Biology

Binding Studies of Metal–Salphen and Metal–Bipyridine Complexes towards G-Quadruplex DNA

Anna Łęczkowska,[a] Jorge Gonzalez-Garcia,[a] Cristina Perez-Arnaiz,[a, b] Begoña Garcia,[b] Andrew J. P. White,[a] and Ramon Vilar*[a]

Abstract: The proposed in vivo formation of G-quadruplex DNA (G4 DNA) in promoter regions of oncogenes and in telomeres has prompted the development of small molecules with high affinity and selectivity for these structures. Herein we report the synthesis of a new di-substituted bipyridine ligand and the corresponding complexes with Ni^{2+} and VO^{2+}. Both these new complexes have been characterized spectroscopically and by X-ray crystallography. Detailed DNA binding studies of these two complexes, together with three previously reported metal salphen complexes, are presented. Using FRET melting assays, the binding affinity and selectivity of the five metal complexes against six different G4 DNA structures as well as a duplex DNA have been determined. In addition, we present detailed ITC and UV/Vis studies to characterize the interaction of the complexes with human telomeric G4 DNA. Finally, we show via a polymerase stop assay that these complexes are able to stabilize a G4 DNA structure (from the *c-Myc* oncogene promoter) and halt the activity of *Taq* polymerase.

Introduction

Besides its canonical double-stranded helix, DNA can fold into a range of different structures such as hairpins, triplexes, cruciform junctions, *i*-motifs and G-quadruplexes (G4).[1] The latter forms from stacks of two or more guanine tetrads that in turn arise from hydrogen bonding network of four guanines (see Figure 1). A large number of putative G-quadruplex forming sequences (ca. 700,000) have been identified in vitro in the human genome[2] and there is increasing evidence they are involved in essential biological processes.[3,4] G-quadruplex-forming sequences in the human genome are found in telomeres[5] and promoter regions of various oncogenes.[6] Consequently, these G4 structures have been proposed as potential targets for therapeutic intervention and therefore significant research has been carried out to develop small molecules with high affinity for G4 DNA.[7–9]

One of the biggest challenges when developing small molecules as quadruplex binders is to make them selective for a given G4 structure over others as well as over duplex DNA. While all G4 structures share some structural features—for example, the stacks of guanine tetrads stabilized by K^+ ions—they show wide structural diversity caused by the strand orientation, base composition, nature of pentose ring, conformation of glycosidic bonds of guanine bases in the G-quartets, length and sequence composition of loops/grooves formed.[10,11]

Initially, most G-quadruplex binding molecules were based on organic heteroaromatic compounds.[12,13] Subsequently, it

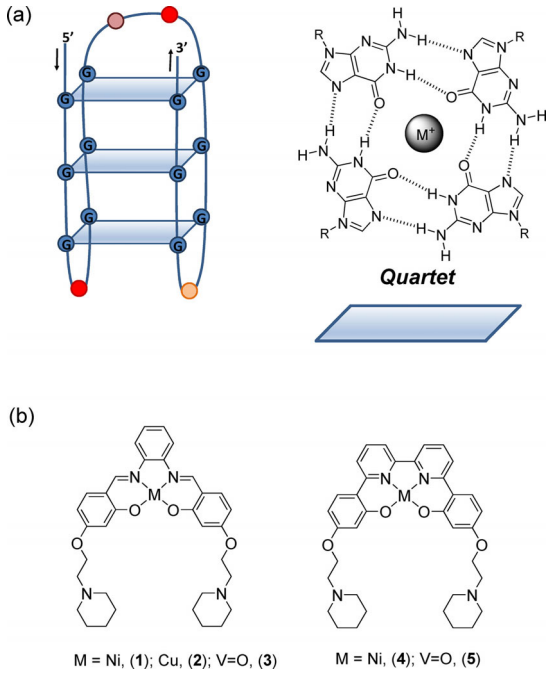

Figure 1. (a) Schematic representation of a G4 DNA structure highlighting the guanine tetrad. (b) Chemical structures of metal-salphen (**1**–**3**) and metal-bipyridine (**4**, **5**) complexes studied in this work.

[a] *Dr. A. Łęczkowska, Dr. J. Gonzalez-Garcia, C. Perez-Arnaiz, Dr. A. J. P. White, Prof. R. Vilar*
Department of Chemistry
Imperial College London
London SW7 2AZ (UK)
E-mail: r.vilar@imperial.ac.uk

[b] *C. Perez-Arnaiz, Prof. B. Garcia*
Universidad de Burgos
Departamento de Química
09001 Burgos (Spain)

Supporting information and the ORCID identification number(s) for the author(s) of this article can be found under: https://doi.org/10.1002/chem.201802248.

was shown that metal complexes can also be excellent G4 DNA binders thanks to their unique electronic and structural features, as has been discussed in detail elsewhere.[14,15] An example of this, are metal salphen and salen complexes, which have been extensively studied over the past 10 years (see Figure 1).[16,17] A wide range of derivatives with different metals (and hence geometries),[18–20] salphen/salen core structure[21,22] and nature/number/position of substituents[19,23–27] have been reported as excellent G4 DNA binders. In spite of this, there is still little information regarding the selectivity of metal-salphens against several different G4 DNA structures.[26]

With the aim of increasing the aromatic planar surface of metal salphens and hence their G4 DNA binding affinity, herein we report the synthesis and structural characterisation of two new metal complexes where Ni^{2+} (**4**) and $[VO]^{+}$ (**5**) are coordinated to a new 6,6′-diphenyl-2,2′-bipyridine ligand (Figure 1). The affinities of these complexes (and of the previously reported metal-salphens **1**–**3**) towards six different G-quadruplex DNA structures have been determined by fluorescence resonance energy transfer (FRET) melting assays. We have also established by detailed isothermal titration calorimetry (ITC) and UV/Vis spectroscopic studies, the affinities and thermodynamic binding parameters for these complexes towards human telomeric G-quadruplex DNA. Finally, using polymerase stop assay (PSA), we report on the ability of these complexes to stabilise the G-quadruplex structure in the promoter region of *c-Myc* and in doing so halt the activity of a polymerase.

Results and Discussion

Design and synthesis of metal complexes

We previously reported the structural characterization of a nickel(II) and a copper(II)-salphen complexes bound to human telomeric G-quadruplex DNA.[17] These structures confirmed that the square planar metal complexes bind to the external G-tetrads via π–π stacking interactions. From these structures, we hypothesized that a system based on a di-substituted bipyridine with four aromatic rings (Figure 1) would have similar dimensions to the salphen ligand but possess an extra phenyl ring which could increase the ability of the resulting metal complexes to interact with the G-tetrad. Besides the polyaromatic tetradentate core of the ligand, we designed the system with two ethyl piperidine substituents analogous to those present in the successful metal-salphen complexes we have previously developed.[16,18] The presence of such substituents is particularly important to increase the compounds' water solubility as well as the affinity towards DNA thanks to the positive charge on the piperidine groups, which are protonated at physiological pH.

Complexes **1**–**3** were synthesized as we previously reported[18] while the new complexes **4** and **5** were prepared as shown in Scheme 1. Several complexes with 6,6′-diphenyl-2,2′-bipyridine ligand derivatives have been reported.[28,29] We therefore adapted some of the previous protocols to prepare our new ligand (**7**) and corresponding metal complexes (**4** and **5**). A Suzuki cross-coupling reaction using 6,6′-dibromo-2,2′-bipyridine and 2,4-dimethoxyphenyl boronic acid was carried out, followed by demethylation with boron tribromide to yield compound **7**. The phenolic scaffold was metalated by using Ni^{2+} or VO^{2+} salts to yield the corresponding metal-bipyridine precursor complexes **8** and **9**, which were then reacted with chloroethyl piperidine to yield the new complexes **4** and **5**. It should be pointed out that no vanadyl complexes with 6,6′-diphenyl-2,2′-bipyridine ligands have been previously reported. All compounds were fully characterized by ^{1}H NMR spectroscopy (except for the vanadyl complexes **5** and **9** which are paramagnetic), mass spectrometry and their purity confirmed by elemental analyses (see Experimental Details). As described in the following section, the X-ray crystal structures of com-

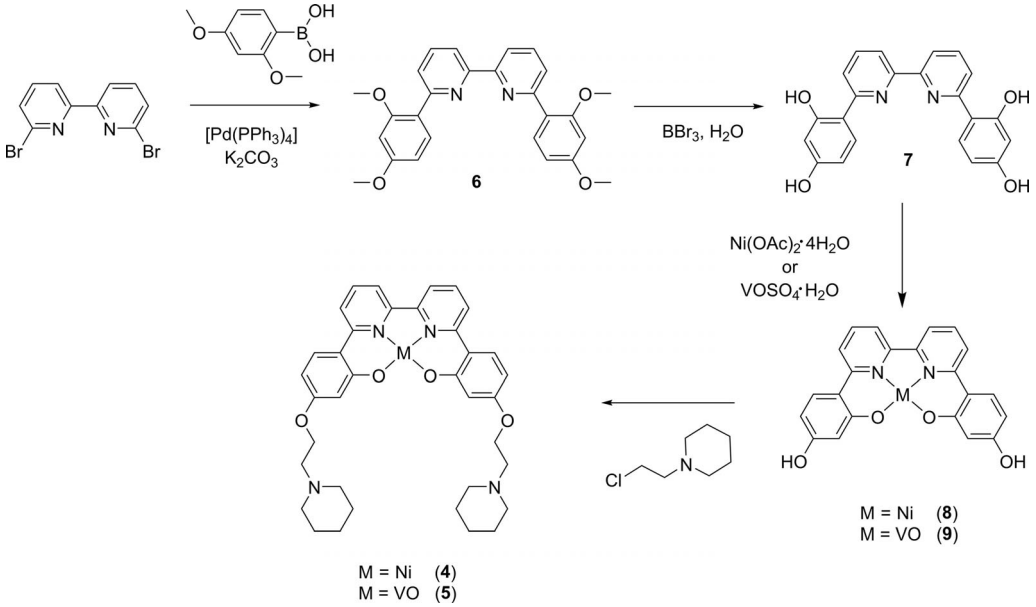

Scheme 1. Synthetic route of bipyridine metal complexes studied in this work.

pounds **4** and **5** were also determined confirming their proposed square planar and square-based pyramidal geometries.

To investigate the ability of the nickel(II) complex **4** to display π–π interactions in solution (and hence its potential to do so with G4 DNA), variable concentration ^{1}H NMR spectroscopic studies were carried out. As has been previously reported, π–π stacking interactions results in shielding of protons and hence in lower ^{1}H NMR chemical shifts in comparison to the non-aggregated species. As can be seen in Figure S12, upon increasing the concentration of the complex all the aromatic signals shifted upfield consistent with the expected increase in π–π interactions.

Similarly, we carried out a variable temperature ^{1}H NMR spectroscopic study of complex **4** (at constant concentration see Figure S13). Upon heating the sample up from 20 to 70 °C, all the aromatic protons shifted. However, in this case two different trends were observed: the resonances between 7.70 and 8.30 ppm all shifted downfield as the temperature increased which is consistent with a decrease of π–π interactions at higher temperature. On the other hand, the resonances between 6.20 and 6.40 ppm (which correspond to the protons next to the O atoms in the di-phenolic ring) shifted upfield. The opposite shift of these signals in comparison to the other aromatic protons reflects a more complex set of intermolecular interactions for the protons in the phenolic ring. It is likely that these two protons display stronger hydrogen bonding interactions with the solvent which decrease as the temperature increases and therefore an upfield shift is observed.

Structural characterisation of 4 and 5

Single crystals of both complexes **4** and **5** suitable for X-ray crystallography were obtained. The four aryl rings in the structure of **4** adopt a distorted conformation (Figure 2); though the bipyridyl unit is relatively coplanar (the torsion angle between rings **A** and **B** being only ca. 2.5°), rings **C** and **D** are noticeably twisted with respect to their adjacent pyridyl rings, the **A–C** and **B–D** torsion angles being around 11.9 and 8.6° respectively. For rings **A** and **C** there is also a significant fold component such that O19 lies ca. 1.00 Å out of the plane of ring **A**. This fold distorts the square planar coordination at the nickel atom such that O14 lies around 0.22 Å out of the (Ni,N1,N7,O29) plane (the atoms of which are coplanar to better than 0.01 Å). Similar distortions from a square planar geometry have been previously observed for other bipyridine bis-phenol nickel(II) complexes.[28]

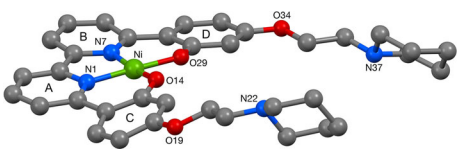

Figure 2. The crystal structure of **4**. Selected bond lengths (Å) and angles (°); Ni–N1 1.877(2), Ni–N7 1.876(2), Ni–O14 1.8317(18), Ni–O29 1.8348(17), N1-Ni-N7 86.75(9), N1-Ni-O14 94.25(8), N1-Ni-O29 178.16(9), N7-Ni-O14 173.46(9), N7-Ni-O29 94.96(8), O14-Ni-O29 84.12(7).

The π-ring systems of adjacent molecules pack across two independent centres of symmetry to form a loosely-linked extended stack along the crystallographic *a* axis direction (Figure 3). The closest approaches are between ring **A** in one

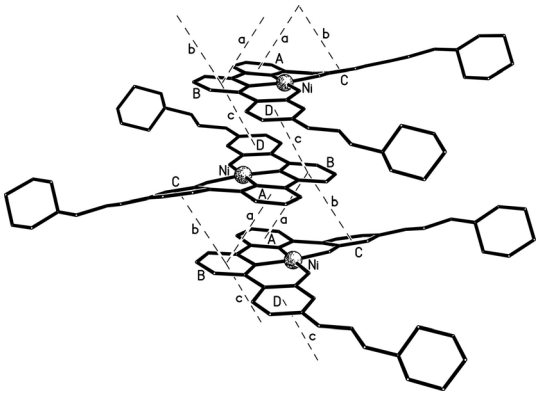

Figure 3. Part of one of the loosely π–π linked stacks of molecules along the *a* axis direction present in the crystal of **4**. Interactions **a**, **b**, and **c** have centroid···centroid and mean interplanar separations (Å) of ca. **a**) 3.90 and 3.44, **b**) 4.00 and 3.33, and **c**) 4.05 and 3.49, the ring pairs being inclined by ca. 3, 21 and 9° respectively.

molecule and ring **B** in the "below" counterpart (centroid···centroid and mean interplanar separations of ca. 3.90 and 3.44 Å, rings inclined by around 3°, interaction **a** in Figure 3), between ring **B** in one molecule and ring **C** in the "below" counterpart (centroid···centroid and mean interplanar separations of ca. 4.00 and 3.33 Å, rings inclined by ca. 21°, interaction **b** in Figure 5), and between ring **B** in one molecule and ring **D** in the "above" counterpart (centroid···centroid and mean interplanar separations of around 4.05 and 3.49 Å, rings inclined by around 9°, interaction **c** in Figure 3).

The four aryl rings in the structure of **5** (Figure 4) adopt a similar distorted conformation to that seen in the related nickel species **4**. The bipyridyl unit is again relatively coplanar with an **A–B** torsion angle of around 3.0°, and rings **C** and **D** are twisted with respect to their adjacent pyridyl rings by approximately 12.3° and 8.3° respectively. For rings **A** and **C** there is again a significant fold component such that O19 here

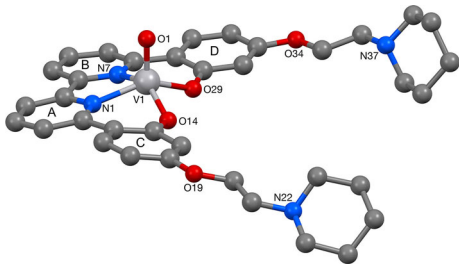

Figure 4. The crystal structure of **5**. Selected bond lengths (Å) and angles (°); V1–O1 1.6012(11), V1–N1 2.0730(12), V1–N7 2.0775(12), V1–O14 1.9095(10), V1–O29 1.9001(11), O1-V1-N1 103.58(5), O1-V1-N7 105.00(5), O1-V1-O14 112.72(5), O1-V1-O29 110.32(6), N1-V1-N7 79.75(5), N1-V1-O14 86.12(5), N1-V1-O29 145.74(5), N7-V1-O14 141.87(5), N7-V1-O29 86.83(5), O14-V1-O29 85.33(4).

lies approximately 0.84 Å out of the plane of ring **A**. Unlike the case with **3**, however, where this fold affects the square planar coordination to the nickel atom, here the square-based pyramidal coordination geometry of the vanadium centre is unaffected; the four basal atoms are coplanar to within 0.03 Å with the metal lying around 0.61 Å out of the basal plane in the direction of the apical atom O1.

The π ring systems of adjacent molecules pack across three independent centres of symmetry to form a sheet of molecules in the crystallographic *ab* plane. Figure S4 in the Supporting Information gives a detailed view of the six π–π interactions around one molecule, whilst Figure 5 here shows part of one

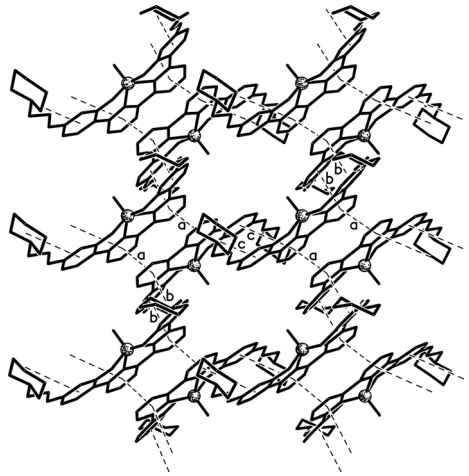

Figure 5. Part of one of the sheets of π–π linked molecules in the *ab* plane present in the crystal of **5**. Interactions **a**, **b**, and **c** have centroid···centroid and mean interplanar separations (Å) of ca. **a**) 3.61 and 3.32, **b**) 3.83 and 3.43, and **c**) 3.93 and 3.39, the ring pairs being inclined by ca. 4, 16 and 8° respectively.

of the resulting sheets. The closest approaches are between ring **A** in one molecule and ring **B** in a *Ci*-related counterpart (centroid···centroid and mean interplanar separations of ca. 3.61 and 3.32 Å, rings inclined by ca. 4°, interaction **a** in Figure 5), between ring **A** in one molecule and ring **C** across an independent centre of symmetry (centroid···centroid and mean interplanar separations of ca. 3.83 and 3.43 Å, rings inclined by ca. 16°, interaction **b** in Figure 5), and between ring **B** in one molecule and ring **D** in the next across another inversion centre (centroid···centroid and mean interplanar separations of ca. 3.93 and 3.39 Å, rings inclined by ca. 8°, interaction **c** in Figure 5).

DNA Affinity: Fluorescence resonance energy transfer (FRET) melting assays

Previously, we have reported that metal-salphen complexes **1**–**3** have high affinity (in particular **1** and **2**) towards human telomeric G-quadruplex DNA and good selectivity over duplex DNA,[16,18] but their binding to a wider range of G-quadruplex structures and therefore their G4-selectivity has not been previously studied. Thus, with the aim of comparing the G4 affinity of **1**–**3** with that of the new complexes **4** and **5** as well as to establish preferences for a given G4 topology, we carried out FRET meting assays with a range of G4 DNA and RNA structures. We studied G-quadruplexes with antiparallel (i.e. 22CTA), parallel (i.e. 25CEB, *c-kit2*, *c-Myc*) as well as mixed/hybrid (i.e. HTelo21 and *Bcl-2*) conformations. Structures HTelo21, 25CEB and 22CTA are derived from telomeric regions while *c-Myc*, *c-kit2* and *Bcl-2* are sequences from oncogene promoter regions. A duplex DNA (ds26) was also studied to investigate the selectivity for G4 vs. duplex DNA (see Experimental Details for details of all sequences).

All metal complexes showed higher affinity for G4 over duplex DNA, with the new complex **4** exhibiting the highest thermal stabilization effect of all complexes under investigation (see Figure 6). Amongst the metal-salphens, complex **1** displayed the highest stabilization for all G4s confirming our previous observations for HTelo21 and *c-Myc* G4 DNA. In the case of HTelo21, two different transitions in the melting curves were clearly observed for the square planar metal complexes **1**, **2** and **4** (see Figures S18, S19 and S21). This suggests more than one binding mode for the square planar complexes with the hybrid HTelo21 structure, which is also consistent with the ITC data discussed in the next section. With regards to the most potent stabilizer **4**, it showed a moderate affinity towards duplex DNA suggesting a possible intercalation of the bipyridine moiety between base-pairs of the double-stranded DNA. Complex **5** showed a similar stabilizing effect on the G-quadruplexes than the most potent salphen complex (**1**) in spite of having a square based pyramidal geometry. This is likely to be due to the more extended π-system in the bipyridine bisphenol ring as compared to salphen which allows the square-based pyramidal complex **5** to display a better G4 DNA affinity than the analogous V-salphen complex **3**.

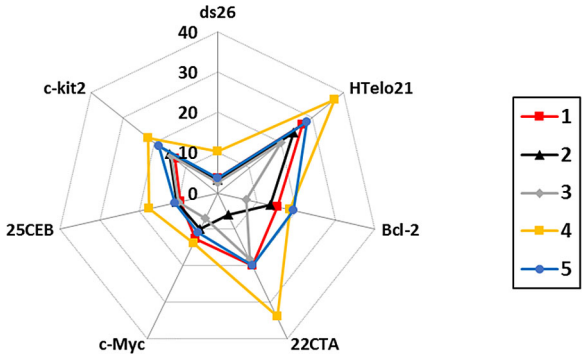

Figure 6. Plot of ΔT_m (radial plot between 0 and 40 °C) of different G-quadruplex DNA structures and one double stranded sequence. Concentration of oligonucleotides = 0.2 μM; concentration of complexes (**1**–**5**) = 1 μM.

The selectivity of **4** for G4 structures was studied by using a competition FRET experiment with non-labeled duplex DNA (ds26). The addition of duplex competitor did not yield any decrease in the melting transition up to 25 equiv. of ds26 (i.e.

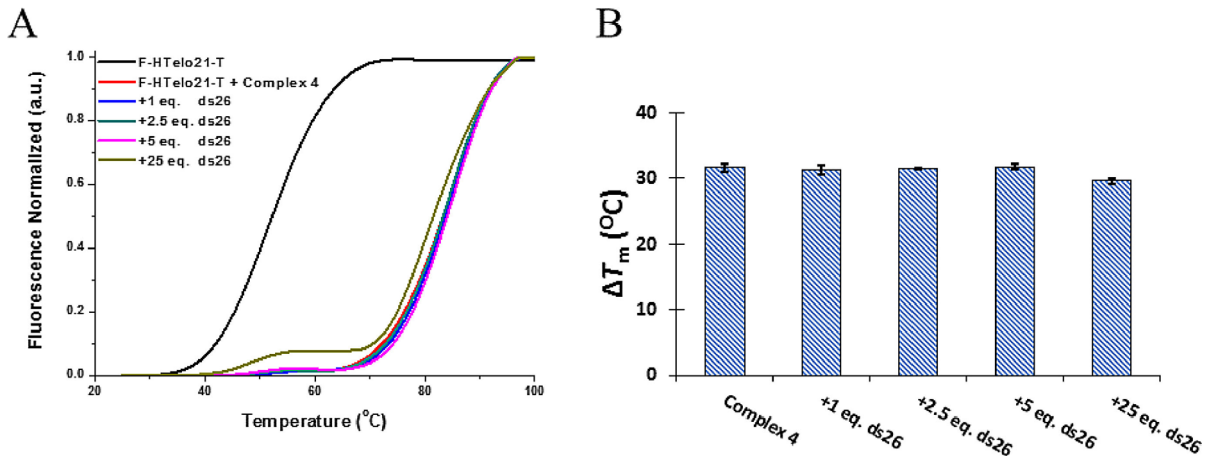

Figure 7. A) Melting curves for F-HTelo21-T with increasing concentrations of ds26 in the presence of 1 μM of complex **4**. B) Variation of the F-HTelo21-T melting temperature with increasing concentrations of unlabelled duplex DNA.

over 250 equiv. of base pairs) suggesting high selectivity for G-quadruplexes over duplex DNA as expected from the previously studied metal-salphen complexes (Figure 7).

DNA binding affinity determined by isothermal titration calorimetry and UV/Vis spectroscopy

The binding affinities (K_a) along with the thermodynamic parameters of the Gibb's equation of complexes **1**–**4** towards human telomeric G-quadruplex DNA were determined using isothermal titration calorimetry (ITC) experiments. The binding isotherms showed one binding event for complex **3**, while for **1** and **2** two binding processes were observed (see Figure 8 and S23 in the Supporting Information). Interestingly, complex **4** displayed three independent binding processes (Figure 10). All the salphen complexes showed binding isotherms consistent with exothermic reactions while for the bipyiridine complex **4**, the first binding event is governed by an endothermic process, while the 2nd and 3rd are exothermic (see Figure 8).

Single site, two-site or three-site binding models[30] were used to obtain the thermodynamic parameters for the interaction between the complexes and human telomeric G4 DNA (Table 1). For compounds **1** and **2,** the first G4 DNA affinity

Table 1. Thermodynamic parameters obtained for the interaction between the metal complexes and human telomeric G4 DNA by ITC at 298 K.

	1	2	3	4
$K_1 \times 10^{-15}$, M^{-1}	270 ± 60	49 ± 5	0.9 ± 0.1	3600 ± 900
ΔH_1, kJ mol^{-1}	−135 ± 3	−99 ± 1	−7.1 ± 0.2	1.2 ± 0.3
$T\Delta S_1$, kJ mol^{-1}	−93.8	−60.4	21.1	50
n_1	3.7 ± 0.8	3.17 ± 0.08	3.33 ± 0.06	1.0 ± 0.3
$K_2 \times 10^{-5}$, M^{-1}	5.7 ± 0.9	1.8 ± 0.9	–	1100 ± 700
ΔH_2, kJ mol^{-1}	−89 ± 3	−161 ± 2	–	−70 ± 10
$T\Delta S_2$, kJ mol^{-1}	−56.3	−131.2	–	−23.5
n_2	8.5 ± 0.6	9.3 ± 0.1		3.8 ± 0.4
$K_3 \times 10^{-5}$, M^{-1}	–	–	–	50 ± 10
ΔH_3, kJ mol^{-1}	–	–	–	−11 ± 1
$T\Delta S_3$, kJ mol^{-1}	–	–	–	12.7 ± 0.9
n_3				8.0 ± 0.7

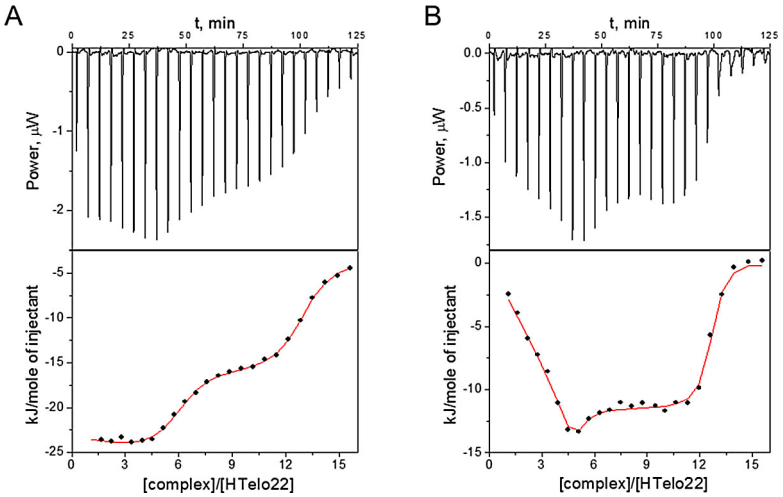

Figure 8. ITC titrations of human telomeric G4 DNA (20 μM) with complexes **1** (A) and **4** (B). The concentration of the respective metal complexes was 1 mM.

constant (K_1) is higher (47 and 27-fold, respectively) than the second one (K_2) (see Table 1) indicating that the first G4 binding site is less hindered than the second. It could be hypothesized that the two binding events correspond to the compounds binding with different affinity to each of the two external G-tetrads in the G4 structure. However, this model is complicated by the observed stoichiometry for the first binding event (see Table 1) which suggests that ca. 3 to 4 molecules of the compounds are needed per G4 DNA structure (see below for further comments on stoichiometry). Both complexes exhibited a higher value of ΔH than $T\Delta S$ indicating that enthalpy is the main driver for the interaction between these complexes and telomeric G4 DNA.

Consistent with the FRET-melting assays and our previous work,[18] the affinity of **3** for G4 DNA is lower than that of **1** and **2**, which can be attributed to the geometries of the complexes: square-based pyramidal for **3** and square planar for **1** and **2**. Interestingly, the binding process for **3** is entropically driven (see Table 1) in contrast to the observations with **1** and **2**. This suggests the possibility of a conformational change of complex **3**, the G4 DNA structure or both upon binding. Taking into account the number of binding processes and the affinity constants obtained, the affinity of the complexes for telomeric G4 DNA follow the trend $\mathbf{3} \ll \mathbf{2} < \mathbf{1} < \mathbf{4}$ which is consistent with the FRET melting assays.

There have been relatively few previous reports where ITC was used to determine the affinities of metal complexes towards G4 DNA.[31–33] One of these studies with metalated porphyrin (TMPyP4), found that Ni^{II}-TMPyP4 and Cu^{II}-TMPyP4 display high affinities to G4 DNA and four independent binding sites,[31] which is similar to our observations. In different study, ITC showed that the binding process (i.e., enthalpy, entropy and number of binding sites) between a Ni^{II}-bis(phenanthroline) complex and telomeric DNA can be affected by the exact choice of telomeric sequence.[32] With HTelo22 (i.e. the same sequence we have used for our studies) it was found that this Ni^{II} complex displayed higher binding affinities than towards the structurally constrained 26-mer sequence.

As indicated above, for the first binding event of complexes **1**–**3**, ca. 3 to 4 equivalents of the respective compound per G4 molecule are needed (see Table 1). A similar behavior has been recently reported for other metal complexes targeting G-quadruplex structures.[34,35] In contrast, complex **4** shows a one-to-one stoichiometry ($n = 1$) for the first binding event although, the subsequent two binding events also show higher ratios. Interestingly, an analogous three-event model with $n = 1$ for the first binding event, has been recently reported for a terpyridine-Cu^{II} complex interacting with G4 DNA.[36] While the number of binding events can be correlated to different sites in the G4 structure (e.g. the two tetrads) it is not clear why the observed stoichiometries are so high for the complexes.

We also studied the possibility that different protonation species could lead to the two-binding process for the interaction of **1** and **2** with HTelo22. Therefore, the basicity of the complexes was examined by means of UV/Vis spectroscopy at different pH values. The overlapping of the absorption spectra

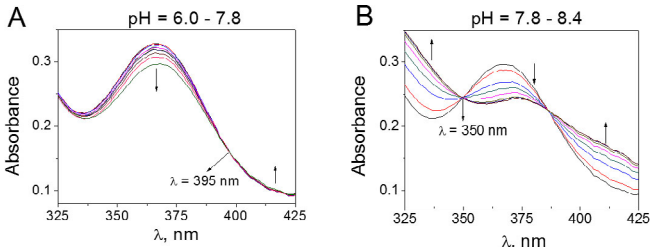

Figure 9. Absorbance spectra of **4** recorded with increasing pH (arrow sense) from 6.0 to 7.8 (A) and from 7.8 to 8.4 (B).

showed two distinct isosbestic points at different pH ranges for **1**–**4** (see Figure 9 for compound **4**), indicating the presence of three different protonated species (see Figures S24–27 in Supporting Information). The pK_a values were obtained by plotting the absorbance versus pH and ranged between 7.6–8.4 (see Supporting Information for all the values) suggesting that the protonation steps occur in the amino group of piperidine rings in good agreement with values in the literature.[37] Thus, these values pointed out that the di-protonated species is the only one present under our experimental conditions and therefore this species should be involved in both binding events with telomeric G4 DNA.

Following on from the results described above, the affinities and binding mode of all metal complexes were studied by using UV/Vis titration experiments. In agreement with the ITC studies, the UV/Vis binding isotherms showed one binding mode for **3** and **5**, two for **1** and **2** and three for **4** (see Figure 10 and Figures S28–S30). It is worth mentioning that the titrations of metal-salphen complexes were already report-

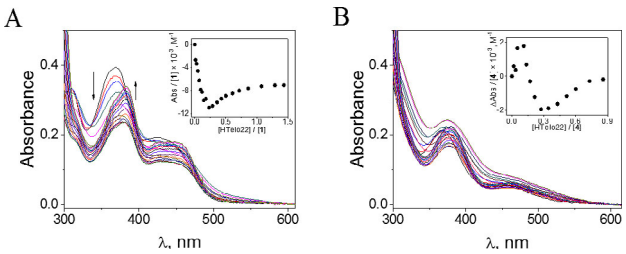

Figure 10. Plots of the UV/Vis titrations of HTelo22 and complexes **1** (A) and **4** (B) ([complex] = 20 μM). Insets are the absorbance binding isotherms (ΔAbs/[complex] vs. [HTelo22]/[complex]) of complex **1** at $\lambda = 370$ nm (A) and **4** at $\lambda = 380$ nm (B) with HTelo22.

ed but reaching lower molar ratios (r = [L]/[G4 DNA] and thus, a second binding process wasn't previously monitored.

The first binding process of the three salphens complexes displayed hypochromism. In the case of **1** and **2**, this was also accompanied by a red-shift of the bands which is consistent with our previous observations, and can be attributed to the π–π stacking interactions of the metal complexes with the guanine tetrad. Interestingly, the second binding event for **1** and **2** showed hyperchromism (and no red shift) which is usually attributed to non-specific interactions such as electrostatic or van der Waals forces.

Complex **4** showed three binding processes: the first and third events resulted in hyperchromism in contrast with the second one that showed hypochromism (Figure S31). Moreover, there is a general red-shift of the spectrum suggesting the stacking between this nickel(II) complex and the guanine tetrad. This data is summarized in Table S3.

Due to the different independent DNA binding sites for the square-planar metal complexes (i.e. **1**, **2** and **4**), it was not possible to fit the UV/Vis titration data to a model from which we could derive the affinity constants for these three complexes. In the case of the square-based pyramidal V=O complexes **3** and **5**, only one binding process was determined by UV/Vis titrations (in agreement with the ITC data previously discussed). Therefore, it was possible to fit the titration data to a 1:1 model and determine the affinity constants for **3** ($\log K_a = 4.97$) and **5** ($\log K_a = 5.11$). The former is consistent with the affinity determined by ITC (i.e. $\log K = 4.95$, see Table 1)

Polymerase stop assay

To test the ability of the complexes to stabilise G-quadruplexes in a functional manner, we performed a Polymerase Stop Assay (PSA) adapted from previously reported protocols.[38,39] A 60 bases-long template oligonucleotide containing a G4-forming sequence derived from *c-Myc* promoter was used as a model for the quadruplex-forming sequences. This was selected since the metal complexes under investigation have an intermediate affinity for this sequence as compared to for example, HTelo G4 and ds26 DNA. This sequence was mixed with a short (22 bases long) labelled oligonucleotide with a sequence complementary to the 3′ overhang of the template. As previously reported, the ability of a polymerase to elongate the labelled-template under different conditions (namely in the presence/absence of K^+ ions or DNA binders) was then studied.

Two control experiments were performed before addition of the compounds to be tested. In the first of these, no K^+ (or compounds) were added to the mixture which led to the full elongation of the primer by the polymerase. In contrast, addition of high concentration of K^+ ions to the mixture and hence formation of G4 DNA in the template sequence led to the appearance of a new band of intermediate size between that of the initial (labelled) primer and the fully elongated one. This indicates that the polymerase is able to extend the primer but only up to the point where the template forms a G4 DNA structure that is, roughly a 40-base long oligonucleotide. Having established this, we then investigated the effect that increasing amounts of the different compounds had on the polymerase activity. As can be seen in Figure 11 and Figure S32–S35, a dose response was observed with the compounds under study. The amount of truncated oligo (i.e. the 40 bases long that stops at the point where the G4 forms on the template strand) could be quantified by analyzing the intensity of the corresponding band in the gel. This clearly became more intense as the corresponding G4 binder concentration increased (see Figure 11 for complex **4** as an example). The intensity of this band was then plotted vs. the concentration of the compound to obtain EC_{50} values (see Figure 11 B). The lowest EC_{50} value (0.92 ± 0.03 μM)—that is, the highest ability to inhibit polymerase mediated by G4 stabilisation—was obtained for complex **4**. This is consistent with the data discussed in previous sections which showed that this compound has the highest affinity for G4 DNA. On the other hand, the highest EC_{50} value (3.8 ± 0.4 μM), and hence lowest activity, was obtained for the square-based pyramidal complex **3**—which is again consistent with the affinity of this compound for G4 DNA as determined by FRET, ITC and UV/Vis studies). Complexes **1** and **2** displayed EC_{50} values of 1.3 ± 0.1 and 1.5 ± 0.2 μM respectively.

Conclusions

The new metal complexes **4** and **5** display high affinity for G4 DNA and selectivity over duplex DNA. As compared to the corresponding metal salphen complexes (i.e. **4** *cf.* **1** and **2**; and **5** *cf.* **3**), both these complexes are better G4 DNA binders—although in the case of complex **4** a modest affinity to duplex DNA is also observed. The selectivity of these five complexes against six different G4 DNA structures of different topology has been studied via FRET melting assays. All of them show a preference towards antiparallel and hybrid conformations over parallel ones.

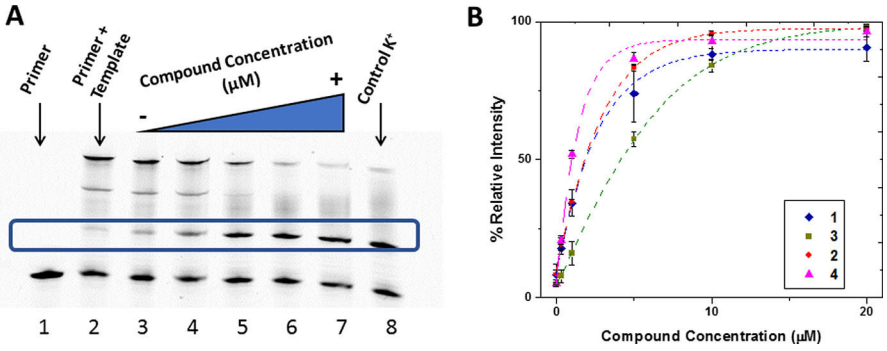

Figure 11. Polymerase Stop Assay (PSA) with a template strand containing the G4-forming sequence from the *c-Myc* gene promoter. (A) Image of the polyacrylamide gel electrophoresis showing the control lanes (1, 2 and 8) as well as the effect of increasing concentration of compound **4** (0.3, 1, 5, 10 and 20 μM) on the product distribution (lanes 3–7). The band corresponding to the pausing product is indicated with a box. (B) Fitting of the experimental data obtained from the PSA with metal complexes **1**–**4**.

To characterise in more detail the interaction between these complexes and G4 DNA, detailed ITC and UV/Vis studies were carried out with HTelo DNA as a representative example of a G-quadruplex structure. The data obtained from these studies is consistent with the FRET melting assays showing that the new complex **4** has the highest affinity for G4 HTelo DNA. On the other hand, as expected, the square-base pyramidal complex **3** has the lowest affinity for G4 DNA. Interestingly, the analogous vanadyl-bipyridine complex **5** with an extra aromatic ring—has significantly higher affinity for G4 than **3** and of roughly the same magnitude than the square planar salphen complexes **1** and **2**. This highlights the importance of π–π stacking in binding to the guanine tetrads. ITC studies have also showed differences in the detailed binding profile of the complexes, with distinct number binding events for the square planar complexes than for the square-based pyramidal ones. Finally, we show that these complexes have the ability to stop the Taq polymerase from elongating a primer when a G4 structure forms in the template strand. The EC_{50} values determined by PSA follow the same trend than the affinity of the metal complexes for G4 DNA.

Experimental Details

Chemicals were purchased from Sigma Aldrich, Alfa Aesar or Acros Organics and used as received. ^1H and ^{13}C NMR spectra were recorded by using a 400 or 500 MHz Bruker Avance Ultrashield NMR spectrometer at 296 K, respectively. Chemical shifts are referenced to residual deuterated solvent. Mass spectra were obtained by using electrospray ionisation (ESI) by Mrs. L. Haigh (Imperial College London) on a LCT Premier Mass Spectrophotometer. IR spectra were recorded on PerkinElmer Spectrum 100 FT-IR Spectrometer. Compounds microanalysis were performed by Mr. A. Dickerson (University of Cambridge). Absorption measurements were made on a PerkinElmer UV/Vis spectrometer. The synthesis of metal-salphen complexes (**1**–**3**) was achieved following a previously reported protocol. 6,6′-dibromo-2,2′-bipyridine was prepared by previously reported procedure.[40]

Synthesis of 6. 6,6′-dibromo-2,2′-bipyridine (0.63 g, 2.0 mmol), 2,4-dimethoxyphenylboronic acid (0.90 g, 5.0 mmol), 2 M aq. K_2CO_3 (10 mL) in THF (50 mL) were stirred under N_2 atmosphere for 30 min. [$Pd(PPh_3)_4$] was then added and the reaction mixture was left stirring at 70 °C for 48 h. After cooling to room temperature, the solution was filtered off and activated carbon was added to the filtrate. The mixture was stirred for further 20 min and then filtered through celite. The solvent was removed under reduced pressure and the compound was taken up with 2 mL of $CHCl_3$. Addition of MeOH (30 mL) afforded a white precipitate. The solid was filtered off and dried under reduced pressure. Yield (0.72 g, 84%). ^1H NMR (400 MHz, $CDCl_3$) $\delta = 8.48$ (dd, $J = 7.7$, 1.0, 1H, H_3), 8.09 (d, $J = 8.6$, 1H, H_{12}), 7.93 (dd, $J = 7.9$, 1.0, 1H, H_5), 7.83 (t, $J = 7.8$, 1H, H_4), 6.72 (dd, $J = 8.6$, 2.4, 1H, H_{11}), 6.62 (d, $J = 2.4$, 1H, H_9), 3.92 ppm (s, 6H, $H_{13,\ 14}$). ^{13}C NMR (100 MHz, $CDCl_3$) $\delta = 161.3$, 158.5, 155.9, 154.6, 136.4, 132.3, 124.5, 122.3, 118.5, 105.3, 98.9, 55.6, 55.5 ppm. MS (ES^+, CH_3Cl) $m/z = 429$ [$M+H^+$]. HRMS (ES+); found: 429.1817, elemental analysis calcd (%) for $C_{26}H_{25}N_2O_4$: 429.1814. EA: found: C 72.69, H 5.59, N 6.76, calcd for $C_{26}H_{24}N_2O_4$: C 72.88, H 5.65, N 6.54; mp. 218–220 °C

Synthesis of 8. Compound **6** (0.11 g, 0.27 mmol) in dry DCM (15 mL) was stirred under nitrogen at −79 °C for 30 min and BBr_3 (0.30 g, 1.2 mmol) was added and stirred overnight at room temperature. The solution was combined with H_2O (20 mL) and the organic phase extracted with CH_2Cl_2 (3×20 mL). The organic phase was evaporated, dried under reduced pressure to afford **7** and used in the following step without further purification. Yield (0.1 g, 98%). MS (ES^+) $m/z = 373$ [M^+]. Crude compound **7** (0.1 g, 0.27 mmol) and $Ni(OAc)_2{\cdot}4H_2O$ (0.07 g, 0.27 mmol) in EtOH (30 mL) were stirred at 60 °C for 3 h during which time a dark red/brown precipitate formed. The solution was then cooled down to room temperature and the precipitate was filtered off, washed with water:EtOH (1:1, 3×15 mL) and dried under reduced pressure. Yield (0.11 g, 92%). ^1H NMR (400 MHz, *[D$_6$]DMSO*) = 9.64 (s, 2H), 8.16 (d, $J = 8.0$, 2H), 8.13–8.00 (m, 4H), 7.78 (d, $J = 9.0$, 2H), 6.22 (d, $J = 2.4$, 2H), 6.16 (dd, $J = 8.9$, 2.5, 2H). MS (ES^+) $m/z = 429$ [M^+].

Synthesis of 9. Compound **6** (0.17 g, 0.41 mmol) in dry CH_2Cl_2 (20 mL) was stirred under nitrogen at −79 °C for 30 min and BBr_3 (0.45 g, 1.8 mmol) was added and stirred overnight at room temperature. The solution was combined with H_2O (20 mL) and the organic phase extracted with CH_2Cl_2 (3×20 mL). The organic phase was evaporated, dried under reduced pressure to afford **6** and used in the following step without further purification. Yield (0.17 g, 98%). MS (ES+) $m/z = 373$ [$M+$]. Crude compound **6** (0.17 g, 0.46 mmol) and $VOSO_4{\cdot}0.5H_2O$ (0.08 g, 0.46 mmol) in MeOH (50 mL) were stirred at 50 °C for 15 h while a dark green precipitate formed. The solution was then cooled down to room temperature, filtered off and the precipitate washed with water (10 mL), MeOH (10 mL) and EtOH (10 mL) and dried under reduced pressure. Yield (0.09 g, 44%). MS (ES^+) $m/z = 438$ [M+H^+]. IR (KBr): $\tilde{\nu} = 1610$ (m), 1555 (m), 1464 (m), 1317 (m), 1180 (m), 1112 (m), 976 (s), 794 cm^{-1} (s).

Synthesis of 4. Compound **8** (0.10 g, 0.23 mmol) and K_2CO_3 (0.06 g, 0.46 mmol) were stirred in dry DMF (30 mL) under N_2 atmosphere for 10 min. 1-(2-chloroethyl)piperidine hydrochloride (0.085 g, 0.46 mmol) was then added and the reaction mixture was stirred at room temperature for 72 h. The solution was concentrated under reduced pressure to ca. 2 mL and water added (50 mL). The red precipitate that formed was filtered off, washed with water (40 mL) and diethyl ether (20 mL) and dried under reduced pressure to give an orange/red powder. Yield: (0.092 g, 62%). Crystals of **4** suitable for X-ray analysis were obtained by slow diffusion of Et_2O into a CH_2Cl_2 solution of the complex. ^1H NMR (400 MHz, *[D$_6$]DMSO*) $\delta = 8.24$ (d, $J = 7.5$ Hz, 1H, H_3), 8.16 (d, $J = 7.7$ Hz, 1H, H_5), 8.10 (t, $J = 7.9$ Hz, 1H, H_4), 7.86 (d, $J = 9.2$ Hz, 1H, H_{12}), 6.35 (d, $J = 2.6$ Hz, 1H, H_9), 6.27 (dd, $J = 9.1$, 2.6 Hz, 1H, H_{11}), 4.07 (t, $J = 5.9$ Hz, 2H, H_{13}), 2.66 (t, $J = 5.9$ Hz, 2H, H_{14}), 2.44 (m, 4H, H_{15}), 1.52 (m, 5H, H_{16}), 1.39 ppm (m, 2H, H_{17}). MS (ES^+, MeOH, $CHCl_3$) $m/z = 651.3$ [M+H^+], 673.2 [M+Na^+]. EA (%): Found: C 62.55, H 5.95, N 7.97; calcd for $C_{36}H_{40}N_4O_4Ni{\cdot}HCl$: C 62.86, H 6.01, N 8.14. IR (KBr): $\tilde{\nu} = 2939$ (w), 1604 (s), 1571 (s), 1536 (m), 1461 (s), 1403 (m), 1234 (m), 1211 (s), 1186 (s), 999 (m) 836 (m), 773 cm^{-1} (m).

Synthesis of 5. Compound **9** (0.10 g, 0.23 mmol), K_2CO_3 (0.06 g, 0.46 mmol) and 1-(2-chloroethyl)piperidine hydrochloride (0.08 g, 0.46 mmol) in dry DMF (20 mL) were stirred at room temperature under N_2 atmosphere for 48 h. The solution was filtered, the filtrate concentrated to ca. 2 mL and water added (50 mL). The precipitate that formed was filtered off, washed with water (30 mL) and diethyl ether (20 mL) and dried under reduced pressure to give a light green powder. The residue was then dissolved in CH_2Cl_2 (3 mL) and the complex was precipitated with *n*-pentane. Yield: (0.064 g, 43%). MS (ES^+, $CHCl_3$) $m/z = 660.3$ [M+H^+]; EA (%): Found: C 62.26, H 5.98, N 8.04; calcd for $C_{36}H_{40}N_4O_5V{\cdot}2H_2O$: C 62.15, H 6.37, N 8.05. IR (KBr): $\tilde{\nu} = 2927$ (w), 1601 (s), 1572 (s) 1544 (m), 1460 (s),

1397 (m), 1353 (m), 1242 (m), 1179 (s), 1116 (m), 1033 (m), 1001 (m), 983 (s), 839 cm^{-1} (m).

X-Ray Crystallography

Crystal data for **4**: $C_{36}H_{40}N_4NiO_4{\cdot}3(H_2O)$, $M=705.48$, triclinic, $P\bar{1}$ (no. 2), $a=9.5217(3)$, $b=11.7214(6)$, $c=15.7343(5)$ Å, $\alpha=93.857(3)$, $\beta=106.015(3)$, $\gamma=96.053(3)^\circ$, $V=1669.97(12)$ Å^3, $Z=2$, $\rho_{cald}=1.403$ g cm^{-3}, $\mu(Cu_{K\alpha})=1.299$ mm^{-1}, $T=173$ K, orange needles, Oxford Diffraction Xcalibur PX Ultra diffractometer; 6452 independent measured reflections ($R_{int}=0.0287$), F^2 refinement,[41,42] R_1(obs) = 0.0486, wR_2(all) = 0.1393, 5167 independent observed absorption-corrected reflections [$|F_o|>4\sigma(|F_o|)$, $2\theta_{max}=145^\circ$], 457 parameters. CCDC 1005613 contains the supplementary crystallographic data for this paper. These data can be obtained free of charge from The Cambridge Crystallographic Data Centre.

Crystal data for **5**: $C_{36}H_{40}N_4O_5V$, $M=659.66$, monoclinic, $P2_1/c$ (no. 14), $a=8.80002(8)$, $b=11.49998(9)$, $c=31.1294(3)$ Å, $\beta=92.3648(8)^\circ$, $V=3147.61(5)$ Å^3, $Z=4$, $\rho_{cald}=1.392$ g cm^{-3}, $\mu(Cu_{K\alpha})=3.047$ mm^{-1}, $T=173$ K, dark orange tabular needles, Oxford Diffraction Xcalibur PX Ultra diffractometer; 6162 independent measured reflections ($R_{int}=0.0233$), F^2 refinement,[41,42] R_1(obs) = 0.0335, wR_2(all) = 0.0943, 5763 independent observed absorption-corrected reflections [$|F_o|>4\sigma(|F_o|)$, $2\theta_{max}=145^\circ$], 444 parameters. CCDC 1005614.

Oligonucleotides and stock solution preparation. Non-labelled oligonucleotides and labelled oligonucleotides of double HPLC-grade purity were purchased from Eurogentec (Belgium). The labelled sequences used were 5′-FAM-dGGG(TTAGGG)3-TAMRA-3′ for telomeric G4 DNA (F-HTelo21-T), 5′-FAM-dTGAGGGTGGGTAGGGTGGGTAA-TAMRA-3′ for *c-Myc*, 5′-FAM-dGGGAGGGCGCTGGGAGGAGGG-TAMRA-3′ for *c-kit2*, 5′-FAM-dAGGGCTAGGGCTAGGGCTAGGG-TAMRA-3′ for 22CTA, 5′-FAM- dAAGGGTGGGTGTAAGTGTGGGTGGGT-TAMRA-3′ for 25CEB, 5′-FAM-dGGGCGCGGGAGGAAGGGGGCGGG-TAMRA-3′ for *Bcl-2* and 5′-FAM-CAATCGGATCGAATTCGATCCGATTG-TAMRA-3′ for ds26 (donor fluorophore FAM, 6-carboxyfluorescein; acceptor fluorophore TAMRA, 6-carboxy-tetramethylrhodamine). The unlabelled oligonucleotides used had the same sequence except for telomeric G4 DNA that 5′-dAGGG(TTAGGG)3-3′ was used (HTelo22).

Tested compounds were dissolved in DMSO to give 10 mM stock solutions. All solutions were stored in 100 μL aliquots at −20 °C, thawed, and diluted immediately before use. Oligonucleotide concentrations were calculated using the following extinction coefficients ε (L cm^{-1} mol^{-1}) at 260 nm given by the supplier: 228500 (HTelo22), 232000 (*c-Myc*), 258900 (ds26), 205600 (c-kit2), 220400 (22CTA), 265100 (25CEB), 231300 (*Bcl-2*) and 220590 (F-HTelo21-T).

Under our experimental conditions the absorbance values were proportional to the metal complex concentrations, thus excluding aggregate formation. Extinction coefficients were calculated in Tris buffer (50 mM) supplemented with 10 mM KCl, pH 7.0, $T=25$ °C. ε (L cm^{-1} м$^{-1}$): 23200 for **1** ($\lambda=370$ nm), 22500 for **2** ($\lambda=380$ nm), 23700 for **3** ($\lambda=322$ nm), 18500 for **4** ($\lambda=290$ nm).

Isothermal Titration Calorimetry (ITC). The ITC experiments were performed at 25 °C with a Nano ITC (TA Instruments, Newcastle, USA). Solutions were degassed in a degassing station (TA, Waters LLC, New Castle, USA) to minimize the formation of bubbles during the titration. In the course of the titration, the compound was injected (25 injections of 2.02 μL) into the calorimetric cell (187 μL) containing the HTelo22 (i.e. dGGG(TTAGGG)$_3$A) solution in 50 mM Tris-HCl, 10 mM KCl at pH 7.0. The stirring speed was maintained constant at 250 rpm. Control experiments were carried out to subtract the contribution of the heat of dilution of the complexes. The resulting thermograms (integrated area of the peak/mole of injectant versus [complex]/[HTelo22] ratio) obtained in the titrations were treated with model equations for single, two or three independent modes of binding using the Nano Analyze Software (TA Instruments, Newcastle, USA).[30] The thermodynamic parameters were obtained from two independent experiments.

UV/Vis spectroscopy. Spectrophotometric measurements were performed with a HP 8453A photodiode array spectrophotometer (Agilent Technologies, Palo Alto, CA) endowed with a temperature control Peltier system. Titrations were carried out by adding increasing amounts of HTelo22 solution (between 0 and 2 equiv) to the complex solution in 1 cm pathlength cells with black quartz sides (50 mM Tris-HCl, 10 mM KCl, pH 7.0, $T=25$ °C). The absorbance data were corrected by the dilution factor. For complexes **3** and **5**, the affinity constants were obtained according to the independent-site model by nonlinear fitting (see details in the Supporting Information).[43] The titrations were performed in triplicate.

FRET melting assays. Doubly labelled and non-labelled oligonucleotides (FAM/TAMRA labelling) were prepared as 20 μM stock solutions in MilliQ water and stock solutions of 0.4 μM were annealed in cacodylate buffer (10 mM, pH 7.4) supplemented with potassium depending on the sequence (*c-Myc*: 1 mM KCl + 99 mM LiCl; HTelo22, 22CTA, *c-kit2*, ds26, 25CEB: 10 mM KCl + 90 mM LiCl; *Bcl-2*: 100 mM KCl). For FRET melting experiments 8-well optical tube strips were used. The final volume of each sample was 40 μL, with a final DNA concentration of 0.20 μM and increasing concentration of tested compound (0–8 μM). Measurements were performed on a PCR Stratagene Mx3005P (Agilent Technologies) with FAM excitation at 450–495 nm and detection at 515–545 nm. Readings were taken from 25 °C to 95 °C every 0.5 °C and at 1 °C min^{-1} melting rate. To obtain melting curves, normalised FAM fluorescence signal was plotted against temperature. From the non-linear fitting of the plot ΔT_m [T_m (with ligand)—T_m (without ligand) obtained from at least three independent measurements] vs. ligand concentration, the ΔT_m value for 1 μM concentration of ligand was obtained. In the case of the competition assays, each well was prepared with a final labelled oligo concentration of 0.20 μM, 1 μM compound, and increasing concentration of non-labelled oligonucleotide to test (0.2, 1 and 2 μM).

Polymerase Stop Assay. The oligonucleotide containing a quadruplex-forming sequence derived from *c-Myc* oncogene (5′-GCGGCTCCTGTGAGGGTGGGGAGGGTGGGGAAGATTCCCGACTTCG-TATTAAGTACTCTAGCCTT-3′) and the corresponding partially complementary FAM label-sequence (5′-FAM-AAGGCTAGAGTACTTAA-TACGA-3′) were used. A mixture of each oligonucleotide (1 μM each) and increasing concentrations of the compounds (0, 0.3, 1, 5, 10 and 20 μM) were annealed in Tris buffer (50 mM, pH 7.4). After cooling to room temperature, the PSA reactions were performed in 1x Taq buffer, containing the previously annealed solution (0.2 μM), dNTPs (0.2 mM), $MgCl_2$ (1.25 mM) and *Taq* DNA polymerase (2.5 U) at 37 °C during 30 min. The reactions were quenched by adding an equal volume of stop buffer (90% formamide, 10 mM NaOH). PSA products were then analysed on a denaturing polyacrylamide gel (20%) in 1x TBE and visualized in FAM dye channel. As a control experiment, the same protocol was followed using the non-forming quadruplex sequence (5′-GCGGCTCCTGTGAGGGTGAA-GAGGGTGGGGA AGATTCCCGACTTCGTATTAAGTACTCTAGCCTT-3′) as a template oligonucleotide.

Acknowledgements

The UK's Engineering and Physical Sciences Research Council (EPSRC) (grant number: EP/H005285/1) is thanked for financial support. J. G.-G. thanks the Royal Society and the British Academy for a Newton Fellowship.

Conflict of interest

The authors declare no conflict of interest.

Keywords: cancer · DNA binding · heterocycles · metal complexes · polymerase

[1] M. Kaushik, M. Kaushik, S. Kaushik, K. Roy, A. Singh, S. Mahendru, M. Kumar, S. Chaudhary, S. Ahmed, S. Kukreti, *Biochem. Biophys. Rep.* **2016**, *5*, 388 – 395.
[2] S. Chambers Vicki, G. Marsico, M. Boutell Jonathan, P. Smith Geoffrey, M. Di Antonio, S. Balasubramanian, *Nat. Biotechnol.* **2015**, *33*, 877 – 881.
[3] D. Rhodes, H. J. Lipps, *Nucleic Acids Res.* **2015**, *43*, 8627 – 8637.
[4] R. Hänsel-Hertsch, M. Di Antonio, S. Balasubramanian, *Nat. Rev. Mol. Cell Biol.* **2017**, *18*, 279 – 284
[5] S. Neidle, *J. Med. Chem.* **2016**, *59*, 5987 – 6011.
[6] R. Hänsel-Hertsch, D. Beraldi, S. V. Lensing, G. Marsico, K. Zyner, A. Parry, M. Di Antonio, J. Pike, H. Kimura, M. Narita, D. Tannahill, S. Balasubramanian, *Nat. Genet.* **2016**, *48*, 1267 – 1272.
[7] S. A. Ohnmacht, S. Neidle, *Bioorg. Med. Chem. Lett.* **2014**, *24*, 2602 – 2612.
[8] S. Neidle, *Nat. Rev. Chem.* **2017**, *1*, 0041.
[9] S. Balasubramanian, L. H. Hurley, S. Neidle, *Nat. Rev. Drug Discovery* **2011**, *10*, 261 – 275.
[10] G. W. Collie, G. N. Parkinson, *Chem. Soc. Rev.* **2011**, *40*, 5867 – 5892.
[11] S. M. Haider, S. Neidle, G. N. Parkinson, *Biochimie* **2011**, *93*, 1239 – 1251.
[12] A. R. Duarte, E. Cadoni, A. S. Ressurreicao, R. Moreira, A. Paulo, *ChemMedChem* **2018**, *13*, 869 – 893.
[13] D. Monchaud, M.-P. Teulade-Fichou, *Org. Biomol. Chem.* **2008**, *6*, 627 – 636.
[14] S. N. Georgiades, N. H. Abd Karim, K. Suntharalingam, R. Vilar, *Angew. Chem. Int. Ed.* **2010**, *49*, 4020 – 4034; *Angew. Chem.* **2010**, *122*, 4114 – 4128.
[15] Q. Cao, Y. Li, E. Freisinger, P. Z. Qin, R. K. O. Sigel, Z.-W. Mao, *Inorg. Chem. Front.* **2017**, *4*, 10 – 32.
[16] J. E. Reed, A. A. Arnal, S. Neidle, R. Vilar, *J. Am. Chem. Soc.* **2006**, *128*, 5992 – 5993.
[17] N. H. Campbell, N. H. A. Karim, G. N. Parkinson, M. Gunaratnam, V. Petrucci, A. K. Todd, R. Vilar, S. Neidle, *J. Med. Chem.* **2012**, *55*, 209 – 222.
[18] A. Arola-Arnal, J. Benet-Buchholz, S. Neidle, R. Vilar, *Inorg. Chem.* **2008**, *47*, 11910 – 11919.
[19] N. H. Abd Karim, O. Mendoza, A. Shivalingam, A. J. Thompson, S. Ghosh, M. K. Kuimova, R. Vilar, *RSC Adv.* **2014**, *4*, 3355 – 3363.
[20] S. Bandeira, J. Gonzalez-Garcia, E. Pensa, T. Albrecht, R. Vilar, *Angew. Chem. Int. Ed.* **2018**, *57*, 310 – 313.
[21] C.-Q. Zhou, T.-C. Liao, Z.-Q. Li, J. Gonzalez-Garcia, M. Reynolds, M. Zou, R. Vilar, *Chem. Eur. J.* **2017**, *23*, 4713 – 4722.
[22] A. Ali, M. Kamra, S. Roy, K. Muniyappa, S. Bhattacharya, *Bioconjugate Chem.* **2017**, *28*, 341 – 352.
[23] A. Terenzi, R. Bonsignore, A. Spinello, C. Gentile, A. Martorana, C. Ducani, B. Hogberg, A. M. Almerico, A. Lauria, G. Barone, *RSC Adv.* **2014**, *4*, 33245 – 33256.
[24] A. Terenzi, D. Loetsch, S. van Schoonhoven, A. Roller, C. R. Kowol, W. Berger, B. K. Keppler, G. Barone, *Dalton Trans.* **2016**, *45*, 7758 – 7767.
[25] P. Wu, D.-L. Ma, C.-H. Leung, S.-C. Yan, N. Zhu, R. Abagyan, C.-M. Che, *Chem. Eur. J.* **2009**, *15*, 13008 – 13021.
[26] L. Lecarme, E. Prado, A. D. Rache, M.-L. Nicolau-Travers, R. Bonnet, A. V. D. Heyden, C. Philouze, D. Gomez, J.-L. Mergny, H. Jamet, E. Defrancq, O. Jarjayes, F. Thomas, *Inorg. Chem.* **2014**, *53*, 12519 – 12531.
[27] V. Rakers, P. Cadinu, J. B. Edel, R. Vilar, *Chem. Sci.* **2018**, *9*, 3459 – 3469.
[28] H. Arora, C. Philouze, O. Jarjayes, F. Thomas, *Dalton Trans.* **2010**, *39*, 10088 – 10098.
[29] Y.-Y. Lin, S.-C. Chan, M. C. W. Chan, Y.-J. Hou, N. Zhu, C.-M. Che, Y. Liu, Y. Wang, *Chem. Eur. J.* **2003**, *9*, 1263 – 1272.
[30] C. A. Brautigam, *Methods* **2015**, *76*, 124 – 136.
[31] J. I. DuPont, K. L. Henderson, A. Metz, V. H. Le, J. P. Emerson, E. A. Lewis, *Biochim. Biophys. Acta Gen. Subj.* **2016**, *1860*, 902 – 909.
[32] C. Musetti, A. P. Krapcho, M. Palumbo, C. Sissi, *PLoS One* **2013**, *8*, e58529.
[33] X.-H. Zheng, Y.-F. Zhong, C.-P. Tan, L.-N. Ji, Z.-W. Mao, *Dalton Trans.* **2012**, *41*, 11807 – 11812.
[34] A. Garci, K. J. Castor, J. Fakhoury, J.-L. Do, J. Di Trani, P. Chidchob, R. S. Stein, A. K. Mittermaier, T. Friscic, H. Sleiman, *J. Am. Chem. Soc.* **2017**, *139*, 16913 – 16922.
[35] L. Hahn, N. J. Buurma, L. H. Gade, *Chem. Eur. J.* **2016**, *22*, 6314 – 6322.
[36] Y. Li, M. Cheng, J. Hao, C. Wang, G. Jia, C. Li, *Chem. Sci.* **2015**, *6*, 5578 – 5585.
[37] A. V. Rayer, K. Z. Sumon, L. Jaffari, A. Henni, *J. Chem. Eng. Data* **2014**, *59*, 3805 – 3813.
[38] L. Ren, A. Zhang, J. Huang, P. Wang, X. Weng, L. Zhang, F. Liang, Z. Tan, X. Zhou, *ChemBioChem* **2007**, *8*, 775 – 780.
[39] H. Han, L. H. Hurley, M. Salazar, *Nucleic Acids Res.* **1999**, *27*, 537 – 542.
[40] J. E. Parks, B. E. Wagner, R. H. Holm, *J. Organomet. Chem.* **1973**, *56*, 53 – 66.
[41] SHELXTL v5.1, Bruker AXS, Madison, WI, **1998**.
[42] SHELX-2013, G. M. Sheldrick, *Acta Crystallogr. Sect. C*, **2015**, *71*, 3 – 8.
[43] F. H. Stootman, D. M. Fisher, A. Rodger, J. R. Aldrich-Wright, *Analyst* **2006**, *131*, 1145 – 1151.

Manuscript received: May 4, 2018
Accepted manuscript online: June 13, 2018
Version of record online: ■■ ■■, 0000

FULL PAPER

G4 Binders: G-quadruplex DNA is emerging as a new target for anticancer agents, which has prompted the development of small molecules with high affinity and selectivity for these structures. Herein a detailed study is reported of the G4 DNA binding properties of five metal complexes and shows their selectivity profile. It is demonstrated that these complexes stabilize G4 DNA and in doing so stop the activity of a polymerase.

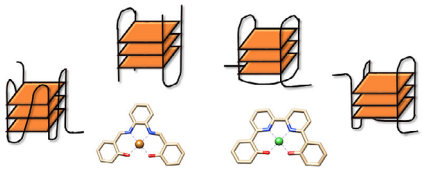

Metal complexes G4-selectivity

Chemical Biology

*A. Łęczkowska, J. Gonzalez-Garcia, C. Perez-Arnaiz, B. Garcia, A. J. P. White, R. Vilar**

■■ – ■■

Binding Studies of Metal–Salphen and Metal–Bipyridine Complexes towards G-Quadruplex DNA